

## MICROSTRUCTURE MODIFICATION OF CEMENT PASTES USING NANOSILICA

DANIEL ŇACHAJ<sup>a,\*</sup>, JIŘÍ NĚMEČEK<sup>a,b</sup>, JIŘÍ NĚMEČEK<sup>a,c</sup>

<sup>a</sup> Czech Technical University in Prague, Faculty of Civil Engineering, Department of Mechanics, Thákurova 7, 166 29 Prague 6, Czech Republic

<sup>b</sup> Ph. D. candidate at CTU in Prague

<sup>c</sup> Associate Professor at CTU in Prague

\* corresponding author: nachadan@fsv.cvut.cz

**ABSTRACT.** The paper describes modifications of cement paste mixtures using nanosilica to affect their physical and chemical properties. Cement pastes from Portland cement CEM I 42.5R with three different substitution ratios of nanosilica 1.5, 3 and 4.5 wt.%/cem. were examined. Micromechanical response and microstructure were characterized using nanoindentation, statistical deconvolution and scanning electron microscopy. About 400 locations were examined on each sample over 40,000  $\mu\text{m}^2$  area. The results indicate an increase of C-S-H phases by 11 vol.% in samples with 4.5 wt.% nanosilica replacement compared to pure Portland cement paste. The increase in C-S-H phases volume was accompanied by the decrease in CH phases by approximately 11 vol.%.

**KEYWORDS:** Nanosilica, nanoindentation, cement paste, C-S-H, image analysis, microstructure.

### 1. INTRODUCTION

Cement has been used as a hydraulic binder for two hundred years. Its composition of inorganic raw materials can solidify, harden and bind other materials. This ability makes it one of the most used building materials. After mixing with water, the cement paste is being formed, which is the basic binding component of concrete. Cement paste is a very complex heterogeneous material that differs in a range of nanoscale to macroscopic dimensions. A mixture of cement particles in water triggers a series of chemical reactions that interact with each other and lead to physical, chemical, and mechanical changes in the system. Products of these reactions are stable hydrated compounds that bind to each other and provide cement with adhesive and cohesive properties [1].

Under various conditions, such as e.g., environmental impacts like carbonation of concrete or impacts caused by the transport of chlorides onto reinforcement's surface, concrete may lose some important properties such as strength or resistance. It can also be impacted by freezing and thawing or impacts of chemical compounds from aggressive environments. Therefore, various additives or admixtures are often used affecting properties, such as: strength, workability, resistance to specific impacts or even the rate of solidification. At present, various admixtures are being used, such as: limestone, fly ash, furnace slag, microsilica, nanosilica (NS), zeolites, and others [2]. The workability of the fresh mixture and the density of cured material are regulated by water-reducing additives. Solidification rate and the development of microstructure can be controlled by accelerators, retarders, crystallisation additives and other substances [3].

Nowadays, nanoparticles have become popular components of cement composites. Their advantages are small size and increased reactivity. Due to their small dimensions, it is possible to achieve transport through a porous concrete system. Nanoparticles can also be used to repair hardened concrete [4]. Dispersion itself might be a problem, but some particles are available in liquid form, which greatly simplifies their usage. Ultrafine particles exhibit unique physical and chemical properties compared to conventional materials. Due to their unique properties, nanoparticles are gaining tremendous attention and are used in many areas to produce new materials. For example, it has been found that the compressive and flexural strength of cementitious mixes has gained an increasing trend by the addition of nanosilica [2, 5, 6]. The incorporation of nanosilica can also increase the strength of the cement paste due to its hydrating effect and high pozzolanic activity, which leads to a higher amount of C-S-H (Calcium Silicate Hydrate) gels and a denser bulk structure due to the reaction of nanosilica with portlandite. However, the disadvantage of cement paste with the addition of nanosilica is that it adversely affects its workability due to its high specific surface area [3].

To study cement microstructure, nanoindentation can be used to determine material parameters such as modulus of elasticity, hardness, plastic or viscous parameters obtained from the indenter load history and penetration depth. The forces involved are on the scale of micronewton, and the depth is on the scale of nanometers. The main advantage compared to classical mechanical tests is that a very small material volume can be accessed with the tip of the nanoindenter [7]. In cementitious composites, hundreds of

indents need to be made to cover the spatial variation of the mechanical properties of their small material phases. By default, the individual indents are spaced several micrometers apart not to influence each other, and large sets of indents (grid) are generally required to cover a representative area of the sample, including all its microstructural constituents in sufficient quantity [8].

The research aims to experimentally examine the influence of nanosilica on the final cement microstructure. The most observed effects include the change in volume representation of individual phases their distribution in the mixture. It is also the mechanical properties of cement paste determined by nanoindentation.

## 2. MICROSTRUCTURE CHARACTERIZATION

Portland cement is composed in an approximate ratio of 5.5:2.5:1:1 mainly from  $C_3S$  (Alite),  $C_2S$  (Belite),  $C_3A$  (Aluminate),  $C_4AF$  (Ferrite). Hydration of Portland cement produces cement paste. The basic hydration chemical reactions include the formation of C-S-H gels and CH (crystalline Calcium Hydroxide) particles, also known as a portlandite which are the main hydration products of cement paste's microstructure (see Fig. 1) and also other phases of cement's microstructure such as: residual clinker, porosity, AFm, AFt and more [1].

The C-S-H gel exists in two mechanically distinct phases, which are referred to hereafter as low- and high-density C-S-H gels. The chemical composition of the paste is not completely constant but may slightly differ from place to place, as well as porosity. Hydration products C-S-H consist of two variations, where one variation is the so-called inner product rich in high-density C-S-H gel (see Fig. 1), developed within the original cement grain boundaries, and outer product created mostly of low-density C-S-H gel mixed with other hydrates, which is formed by storage in an originally water-filled space [9].

To modify the microstructure, it is suitable to use nanosilica, which is chemically compatible with cement and can be produced relatively easily. In addition to creating nucleation sites to produce C-S-H gels arising from reaction with CH, nanosilica can also act as a nano-filler, which reduces the nano and microporosity of concrete [1, 10].

When applying nanoparticles, the problem of particle aggregation is often encountered. Nanoparticles easily aggregate due to their high surface tension and large amount, so their even distribution can be a problem [11].

## 3. NANOINDENTATION

The main advantage compared to mechanical tests at the macro level is that the tip of the indenter can gain access to very small volumes of material and their

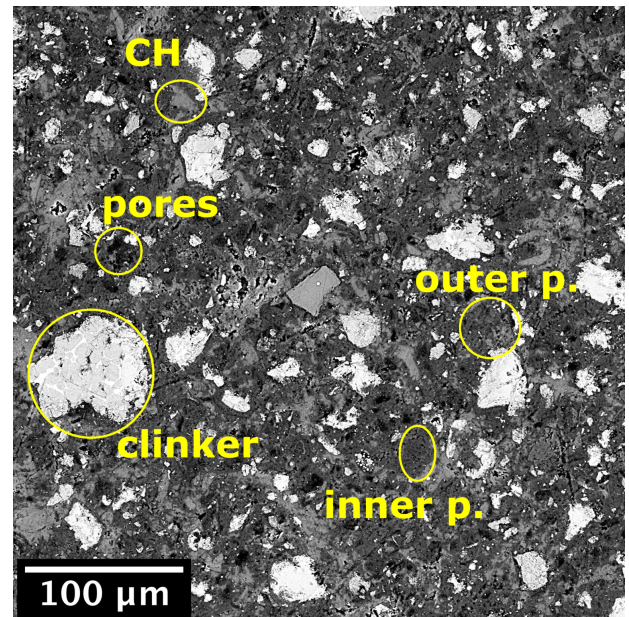


FIGURE 1. SEM photo of cement paste showing phases.

properties in the nanometre range. The principle of nanoindentation consists in pressing a very small tip with certain properties (material and geometry) into the surface of specimen, which then creates an indent. This makes it possible to obtain different material parameters such as: modulus of elasticity, hardness, plastic, and viscous parameters.

The nanoindentation itself can also be affected by unwanted influences such as imperfectly polished surfaces containing scratches or even not completely clean surfaces where even a small dust particle attached to the tip of the indenter can affect the measurement. Errors will be more pronounced for the phase with a lower abundance than for the phase with a higher abundance.

Oliver and Pharr (1992) proposed a method for determining the reduced modulus of elasticity based on the contact depth of the indent [12]. It is based on the general relationships derived by Sneddon for loading, unloading and contact surface for an indent, which can be described as a solid of revolution of smooth functions. Sneddon proved that the load-displacement relationships can be described by the following function[13]:

$$P = \alpha h^m, \quad (1)$$

where  $P$  is the indenter load,  $h$  is the displacement,  $m$  is the shape parameter ( $m = 1$  for flat cylinder,  $2$  for cone and  $1.5$  for sphere) and  $\alpha$  is the material constant.

The reduced modulus  $E_r$  is evaluated from the unloading curve by Oliver-Pharr method [12].

$$E_r = \frac{1}{\beta} \frac{\sqrt{\pi}}{2} \frac{S}{\sqrt{A_c}}, \quad (2)$$

where  $\beta$  is the geometric constant (1.034 for Berkovich tip [8]),  $S$  is an initial unloading stiffness and  $A_c$  is

the projected contact area of the indenter at the peak of loading. The function is calibrated on fused quartz.

The Young's modulus of investigated material can be determined using the relation:

$$\frac{1}{E_r} = \frac{(1 - \nu^2)}{E} + \frac{(1 - \nu_i^2)}{E_i}, \quad (3)$$

where  $E$  is the Young's elastic modulus of the material,  $\nu$  is Poisson's ratio of the material (0.2 for cement paste [8]),  $E_i$  is the elastic modulus of the indenter tip and  $\nu_i$  is the Poisson's ratio of the indenter tip ( $E_i=1141$  GPa and  $\nu_i=0.07$  for diamond [8]).

The output of each indent is a curve showing the applied force and the depth of the indent. From this curve, Young's modulus can be calculated using the above relations.

#### 4. IMAGE ANALYSIS

Image analysis is used for observation and subsequent preparation of cement paste phases. The observed parameters are e.g. the size of the phases, their representation and, where appropriate, their shape. Images are made in a gray range (0-255) of colors, and the colors of pixels vary according to the density of the physical element. The darker colored pixel in the SEM-BSE image represents elements with a lower proton number, while the lighter colored pixel, on the other hand, represents areas with elements with a higher proton number [14].

It is important to select an adequate gray-level threshold for extracting individual objects when processing an image. Various techniques have been proposed in this regard. Ideally, the histogram has a deep and sharp valley between two peaks representing objects, so choosing a threshold at the bottom of this valley is possible. However, it is often difficult for most images to accurately detect the bottom of a valley, especially when the valley is flat and wide, full of noise, or when the two peaks are extremely different in height and often without creating a detectable valley.

In computer vision and image processing, the Otsu method is used to perform automatic image thresholding, whose algorithm in its simplest form returns a single intensity threshold that separates pixels into two classes. Using this method, pixels can be separated into several classes. In this method, the image is viewed as two groups of points with different ranges of intensity values. The problem is that these intensity ranges usually overlap, and therefore the method seeks to minimize misidentification of pixels [15].

The color of the pixels varies according to the density of the physical element. A darker colored pixel represents lower density elements, while lighter elements represent a higher density area. The sizes of the individual phases reach dimensions in the order of tens of micrometers [9]. Thus, the chosen area should ensure a sufficiently representative volume of samples (RVE) [16].

### 5. EXPERIMENTAL PART

#### 5.1. SAMPLE PREPARATION

Four types of cement paste samples were produced, three of them with different proportions of nanosilica and one reference sample without nanosilica. The cement used for this purposes was CEM I 42,5R (Radotín, Českomoravský, a.s.). Part of the cement was replaced by nanosilica in three proportions, precisely: 1.5 wt.%, 3 wt.% and 4.5 wt.%. Major substitutions have not been made based on the available literature, as in some cases, its have been proved counterproductive in terms of pore growth [5]. The addition of nanosilica was performed using an Akzo Nobel Levasil CB8, which is a colloidal solution of nano-SiO<sub>2</sub> with the following properties: density = 1.4 g/cm<sup>3</sup>, solid particle content = 50 %, H<sub>2</sub>O = 50 %, particle size = 20 - 250 nm and pH = 9.5. The cement slurry was placed in cylindrical plastic ampules with a base diameter of 27 mm and a cylinder height of 70 mm. The following day, the hardened samples were demoulded, stored in water and labeled as follows (see Tab 1), where NS representation is the ratio of NS weight to cement weight in percentage:

Label	NS/CEM [wt%]	CEM [g]	Water [g]	CB8 [g]	w/b [-]
CNS00	0.0	300.0	120.0	0.0	0.4
CNS15	1.5	298.1	116.6	8.9	0.4
CNS30	3.0	293.7	112.2	17.6	0.4
CNS45	4.5	289.5	108.0	26.1	0.4

TABLE 1. Labelling of individual samples with the specific weights of the additives.

where C represents cement, NS represents nano-SiO<sub>2</sub>, CB8 is the label for Akzo Nobel Levasil CB8, w is water and b is a binder which is the sum of CEM and NS.

To examine samples at a specific point in the aging process was hydration stopped at 28 days by placing samples in acetone for approximately 30 days. Subsequently, samples were dried in a dryer for one day at a temperature 50 °C.

For possible observation, the surface of the samples was treated, where the samples were polished with a Struers Tegramin 20 polisher. The polishing process was the same for all samples. The samples were polished with silicon carbide papers with grit sizes of 1200, 2000 and 4000. The samples were placed in a glass flask with technical alcohol and placed in an ultrasonic cleaner for two minutes between each polishing step. Finally, the samples were manually polished with a diamond suspension with a particle size of 0.25 µm on a fine cloth disk Struers MD-Dac and subsequently cleaned in an ultrasonic cleaner.

#### 5.2. SEM ANALYSIS

Prepared samples were observed by SEM Phenom XL from which outputs (BSE images) were subjected to

the image analysis necessary to perform representation of individual phases. The size of the examined area of one BSE image from which the image analysis was performed is  $746 \times 746 \mu\text{m}$  for  $360\times$  magnification and  $384 \times 384 \mu\text{m}$  for  $700\times$  magnification. The magnifications were chosen to cover the phases and their transitions, as the phase sizes reach tens of micrometers [9]. For each sample, 20 images were taken from a  $360\times$  magnification and also 20 images from a  $700\times$  magnification. Thus, a total of 40 images were taken, representing an area of  $14.08 \text{ mm}^2$ .

The basis of image analysis is, in addition to the correct preparation of samples, also the correct choice of the thresholds of individual phases. Thresholding was performed using MATLAB software based on the Otsu method mentioned above, which is predefined in the program. The threshold value of some images was manually adjusted due to the different contrast and brightness of the images and also due to scratches and an inaccurate amount of pore growth.

### 5.3. NANOINDENTATION

The most suitable area was selected for each sample with the least possible occurrence of defects caused during polishing and with the smallest possible occurrence of pores. The size of the matrix created by indents for each sample was  $200 \times 200 \mu\text{m}$ .

Nanoindentation was gradually performed using the CSM Instruments device. Samples were probed by a cube-corner tip. The trapezoidal loading diagram was as follows: with a loading rate  $24 \text{ mN/min}$ , the maximum force of  $2 \text{ mN}$  was reached after 5 seconds, where began 20 second holding phase, followed by 5 s linear unloading at the same rate. Totally 400 indents ( $20 \times 20$  grid) with an axial distance of  $10 \mu\text{m}$  between the indents were made for each sample.

## 6. RESULTS AND DISCUSSION

### 6.1. RESULTS OF IMAGE ANALYSIS

Microscope images show us that the addition of NS causes a change in the volume representations of individual phases. It is possible to see scratches in the images caused by imperfect polishing (see Fig. 2, 3). These scratches slightly increase the percentage of pores, which, however, should not significantly impact the results from a statistical point of view.

Statistically, the representation for a magnification of  $700\times$  is similar to a magnification of  $360\times$ . At both magnifications, a decrease in the incidence of portlandite and an increase in the incidence of C-S-H can be observed in the same way. That was the reason for merging these magnifications into one group.

A clear trend can still be seen where  $4.5 \text{ wt}\%$  of nanosilica increases the proportion of C-S-H phases in the samples by about  $7\%$ ,  $3 \text{ wt}\%$  by approximately  $3.5\%$  and  $1.5 \text{ wt}\%$  by about  $3\%$  (see Tab. 2 and Fig. 5). The increase in the incidence of samples with the addition of nanosilica could be attributed to NS, which

reacts with CH in the presence of water and thus contributes to the production of C-S-H. The increase in the C-S-H phase was accompanied by a decrease in the CH phase by approximately  $5\%$  for  $4.5 \text{ wt}\%$  of nanosilica,  $3\%$  for  $3 \text{ wt}\%$  of nanosilica and about  $1\%$  for  $1.5 \text{ wt}\%$  of nanosilica, see Tab. 2 and Fig. 5. Regarding pores, a significant reduction can also be observed in samples with a higher nanosilica content.

### 6.2. RESULTS OF NANOINDENTATION

Every sample was subjected to 400 indents where a load-displacement curve was made for each indent, see Fig. 4. Subsequently, the clinker phases ( $E > 45 \text{ GPa}$ ) and the low stiffness phases ( $E < 17 \text{ GPa}$ ) were separated due to the great variability in which a large statistical error could occur [7]. The values from the indentations in the clinker region varied widely, which is due both to their composition, where unhydrated clinker residues tend to contain  $\text{Al}_2\text{O}_3$ , which substantially increased the measured values, but also to their position and orientation relative to the tip of the indenter, where the individual particles have different Young's moduli in different directions of the force application. In addition to the orientation of the particle itself towards the indenter tip, Young's modulus is also affected by the compliance of the surroundings.

The distribution of elastic moduli was calculated with the aid of deconvolution, where all data whose Young's modulus of elasticity ranges from  $17 \text{ GPa}$  to  $45 \text{ GPa}$  were deconvoluted into two phases, namely C-S-H and CH phases [7]. The distribution of the individual Young's modules of certain phases from which the volume representation was subsequently made can be observed in Table 3, from which it is possible to observe that the nanosilica with a high probability does not affect Young's modulus as affect volume representation of certain phases. Based on this distribution, a table (see Tab. 4) representing the percentages of each phase was then evaluated.

An increase in the C-S-H phase of approximately  $5\%$  was also observed for samples with the addition of  $3 \text{ wt}\%$  of NS with an equal decrease in the CH phase and an increase of approximately  $3\%$  for samples with the addition of  $1.5 \text{ wt}\%$  of NS also with an equal decrease in the CH phase (see Tab. 4). The finding can be observed for samples with NS addition, where samples with higher NS content usually contain more C-S-H, which is attributed to the reaction of NS with CH.

### 6.3. MUTUAL COMPARISON

On the positive side, the results from nanoindentation copy the results from image analysis, which to some extent confirms the trend of the behavior of the samples with NS addition. A comparison of the results of the percentage volume representations from the two experimental techniques can be observed in Fig. 5 where the results from image analysis were converted from four phases (pore, C-S-H, CH, clinker) to two

Label	C-S-H [%]	Increase C-S-H [%]	CH [%]	Increase CH [%]	Clinker [%]	Increase Clinker [%]	Pores [%]	Increase Pores [%]
CNS00	60.5 ± 1.3	±0.0	18.3 ± 2.1	±0.0	10.4 ± 1.4	±0.0	10.8 ± 2.1	±0.0
CNS15	63.4 ± 2.7	+2.9	17.1 ± 2.3	-1.2	10.8 ± 1.9	+0.4	8.7 ± 2.6	-2.1
CNS30	63.5 ± 1.7	+3.5	15.6 ± 1.8	-2.7	13.6 ± 2.0	+3.2	7.3 ± 2.3	-3.5
CNS45	67.8 ± 2.7	+7.2	13.1 ± 1.1	-5.2	13.6 ± 1.6	+3.2	5.4 ± 0.9	-5.4

TABLE 2. Volume representations of individual phases obtained from image analysis.

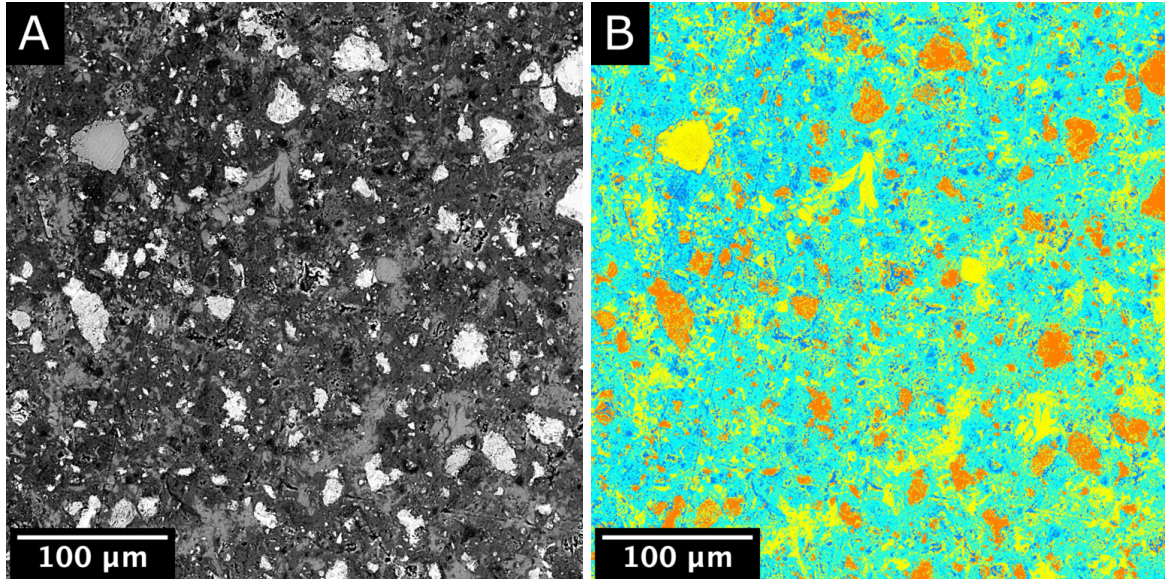


FIGURE 2. A) SEM photo of sample CNS00 B) marked phases after image analysis, where blue color represents pores, yellow portlandite, orange clinker, green HD C-S-H and turquoise LD C-S-H.

Label	C-S-H $E$ [GPa]	CH $E$ [GPa]
CNS00	30.3 ± 1.7	39.2 ± 2.5
CNS15	30.7 ± 2.7	40.1 ± 2.5
CNS30	26.7 ± 3.8	37.8 ± 2.9
CNS45	29.6 ± 4.0	41.1 ± 2.0

TABLE 3. Distribution of Young's modulus of individual phases.

Label	C-S-H [%]	Increase C-S-H [%]	CH [%]	Increase CH [%]
CNS00	74.9	±0.0	25.1	±0.0
CNS15	77.8	+2.9	22.2	-2.9
CNS30	80.2	+5.3	19.8	-5.3
CNS45	85.9	+11.0	14.1	-11.0

TABLE 4. Volume representations of individual phases obtained from nanoindentation.

phases (C-S-H, CH). The reduction from four phases to two phases was made in order to be able to compare the techniques since only two phases were evaluated by nanoindentation.

It is also important to note that the area of the sample examined by nanoindentation is 0.04 mm<sup>2</sup>. The area of the sample examined by image analysis is an order of magnitude higher, namely 14.08 mm<sup>2</sup>,

which may also play a role in comparing the results.

## 7. CONCLUSIONS

This paper focuses on the modification of the microstructure and nanomechanical properties of cement paste using nanoparticles. The most important conclusions of the work can be summarized in the following four points:

- Based on the results from image analysis and nanoindentation, it can be said that replacing cement with nano-silica leads to an increase in the volume of C-S-H gels in this experiment. For samples with 4.5 wt% of NS aged 28 days, approximately by 7% compared to the pure cement paste sample according to image analysis and approximately by 11% according to nanoindentation.
- The increase in the C-S-H phase was accompanied by a decrease in the CH phase. By nanoindentation, it was found that the decrease of C-S-H phase for samples with 4.5 wt% of NS was approximately by 11%, where by image analysis, a decrease of approximately by 5% was recorded. The difference in the two methods is due to the area studied and the fact that two phases were produced by nanoindentation and four by image analysis. On the positive side, the trend for both techniques is favorable.

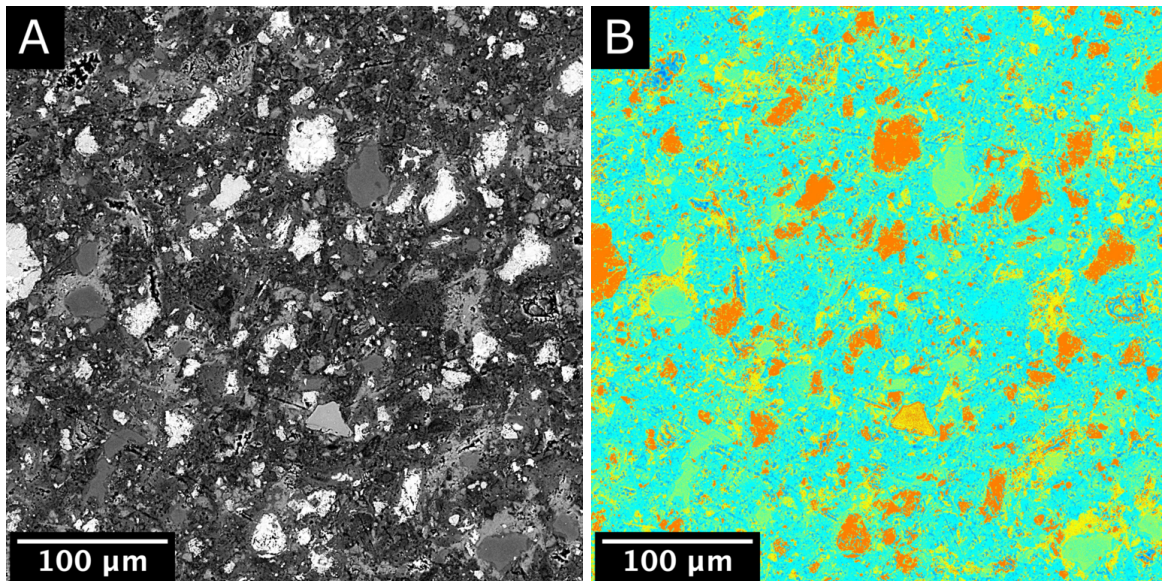


FIGURE 3. A) SEM photo of sample CNS45 B) marked phases after image analysis, where blue color represents pores, yellow portlandite, orange clinker, green HD C-S-H and turquoise LD C-S-H.

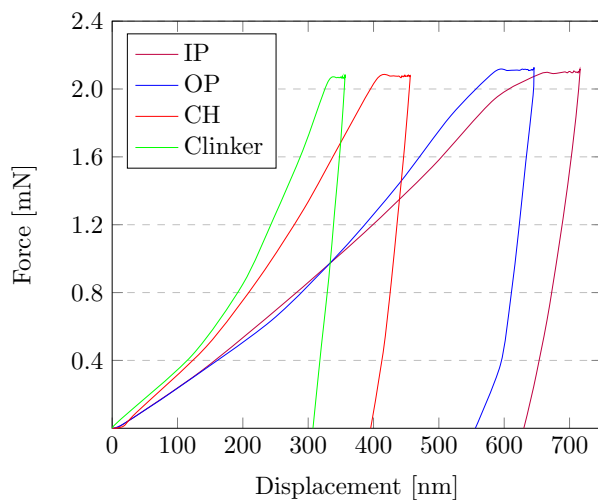


FIGURE 4. Typical indentation load-displacement curves, where OP is outer product and IP is inner product.

- The volume fraction of low-stiffness phases and clinker obtained by nanoindentation is difficult to determine because the fraction of these phases is small or easily influenced by other phases.
- It can be concluded that the RVE for image analysis is large enough, as the results from 360x magnification were very similar to those from 700x magnification. However, the image analysis revealed an unexpected trend of increasing clinker phase in the samples with the NS addition, which may be due to incorrectly determined thresholding.

#### ACKNOWLEDGEMENTS

Financial support of the Czech Science Foundation (project No. 21-11965S) and the Grant Agency of the Czech Technical University in Prague (SGS20/107/OHK1/2T/11) are

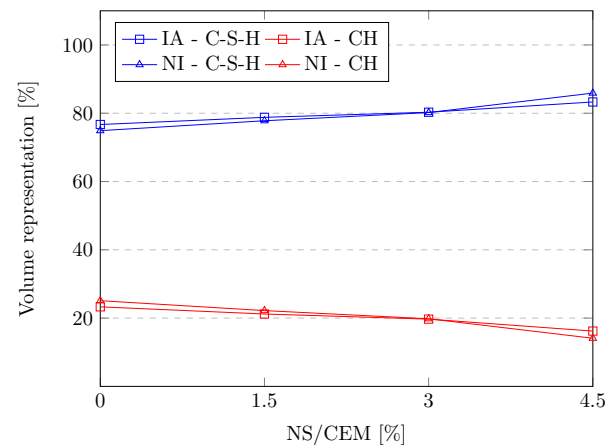


FIGURE 5. Volume representations of a given phases, where IA is image analysis NI si nanoindentation.

gratefully acknowledged.

#### REFERENCES

- [1] F. Sanchez, K. Sobolev. Nanotechnology in concrete – a review. *Construction and Building Materials* **24**(11):2060 – 2071, 2010. <https://doi.org/10.1016/j.conbuildmat.2010.03.014>.
- [2] G. H. Barbhuiya, M. A. Moiz, S. D. Hasan, M. M. Zaheer. Effects of the nanosilica addition on cement concrete: A review. *Materials Today: Proceedings* **32**:560–566, 2020. 3rd International Conference on Innovative Technologies for Clean and Sustainable Development, <https://doi.org/10.1016/j.matpr.2020.02.143>.
- [3] S. Kawashima, P. Hou, D. J. Corr, S. P. Shah. Modification of cement-based materials with nanoparticles. *Cement and Concrete Composites* **36**:8–15, 2013. Special issue: Nanotechnology in Construction, <https://doi.org/10.1016/j.cemconcomp.2012.06.012>.
- [4] J. Němeček, R. Šulc, J. Němečková, J. Kruiš. Nanoparticles in concrete: Application in fresh and hardened

- state. *Key Engineering Materials* **760**:3–9, 2018.  
<https://doi.org/10.4028/www.scientific.net/KEM.760.3>.
- [5] R. Yu, P. Spiesz, H. Brouwers. Effect of nano-silica on the hydration and microstructure development of ultra-high performance concrete (uhpc) with a low binder amount. *Construction and Building Materials* **65**:140–150, 2014.  
<https://doi.org/10.1016/j.conbuildmat.2014.04.063>.
- [6] G. Quercia, P. Spiesz, G. Hüsken, H. Brouwers. Scc modification by use of amorphous nano-silica. *Cement and Concrete Composites* **45**:69–81, 2014.  
<https://doi.org/10.1016/j.cemconcomp.2013.09.001>.
- [7] J. Němeček. *Nanoindentation of Heterogeneous Structural Materials*, vol. 14. Habilitation thesis, CTU Reports, Czech Technical University in Prague, 2010, ISBN 978-80-01-04501-5.
- [8] J. Němeček, J. Lukeš, J. Němeček. High-speed mechanical mapping of blended cement pastes and its comparison with standard modes of nanoindentation. *Materials Today Communications* **23**:100806, 2020.  
<https://doi.org/10.1016/j.mtcomm.2019.100806>.
- [9] S. Diamond. The microstructure of cement paste and concrete—a visual primer. *Cement and Concrete Composites* **26**(8):919–933, 2004. Scanning electron microscopy of cements and concretes,  
<https://doi.org/10.1016/j.cemconcomp.2004.02.028>.
- [10] T. Ji. Preliminary study on the water permeability and microstructure of concrete incorporating nano-sio<sub>2</sub>. *Cement and Concrete Research* **35**(10):1943–1947, 2005.  
<https://doi.org/10.1016/j.cemconres.2005.07.004>.
- [11] H. Li, H. gang Xiao, J. Yuan, J. Ou. Microstructure of cement mortar with nano-particles. *Composites Part B: Engineering* **35**(2):185–189, 2004. Nanocomposites,  
[https://doi.org/10.1016/S1359-8368\(03\)00052-0](https://doi.org/10.1016/S1359-8368(03)00052-0).
- [12] W. C. Oliver, G. M. Pharr. An improved technique for determining hardness and elastic modulus using load and displacement sensing indentation experiments. *Journal of materials research* **7**(6):1564–1583, 1992.  
<https://doi.org/10.1557/JMR.1992.1564>.
- [13] I. N. Sneddon. The relation between load and penetration in the axisymmetric boussinesq problem for a punch of arbitrary profile. *International journal of engineering science* **3**(1):47–57, 1965.  
[https://doi.org/10.1016/0020-7225\(65\)90019-4](https://doi.org/10.1016/0020-7225(65)90019-4).
- [14] A. Luis, L. Deng, L. Shao, H. A. Li. Triaxial behaviour and image analysis of edmonton clay treated with cement and fly ash. *Construction and Building Materials* **197**:208–219, 2019.  
<https://doi.org/10.1016/j.conbuildmat.2018.11.222>.
- [15] N. Otsu. A threshold selection method from gray-level histograms. *IEEE transactions on systems, man, and cybernetics* **9**(1):62–66, 1979.
- [16] J. Němeček, V. Králík, J. Vondřejc. Micromechanical analysis of heterogeneous structural materials. *Cement and Concrete Composites* **36**:85–92, 2013. Special issue: Nanotechnology in Construction,  
<https://doi.org/10.1016/j.cemconcomp.2012.06.015>.